Angewandte Chemie International Edition

Angewandte International Edition Chemie GDCh German Chemical Society

How to cite: *Angew. Chem. Int. Ed.* **2026**, 65, e25787
doi.org/10.1002/anie.202525787

RESEARCH ARTICLE OPEN ACCESS

π-Enlargement in Porphyrin Macrocycles at Interfaces

Ana Barragán[1] | Elena Pérez-Elvira[1] | Alba García-Frutos[1] | Diego J. Vicent[2] | Pingo Mutombo[3] | Koen Lauwaet[1] | José M. Gallego[4] | Rodolfo Miranda[1] | José I. Urgel[1,5] | Aurelio Gallardo[1] | Nazario Martín[1,2] | David Écija[1,5]

[1]IMDEA Nanoscience, C/ Faraday 9, Campus De Cantoblanco, Madrid, Spain | [2]Departamento De Química Orgánica, Facultad de Ciencias Químicas, Universidad Complutense, Madrid, Spain | [3]Institute of Physics of the Czech Academy of Science, Praha, Czech Republic | [4]Instituto De Ciencia de Materiales de Madrid (ICMM), CSIC, Cantoblanco, Madrid, Spain | [5]Unidad De Nanomateriales Avanzados, IMDEA Nanoscience, Unidad asociada Al CSIC Por El ICMM, Madrid, Spain

Correspondence: Ana Barragán (ana.barragan@imdea.org) | Aurelio Gallardo (aurelio.gallardo@imdea.org) | Nazario Martín (nazmar@ucm.es) | David Écija (david.ecija@imdea.org)

Received: 21 November 2025 | **Revised:** 28 February 2026 | **Accepted:** 24 March 2026

Keywords: antiaromaticity | on-surface synthesis | porphyrin chemistry | scanning probe microscopy

ABSTRACT

Porphyrins are essential heteroatomic macrocycles, fundamental to both biological systems and advanced technology. Their unique molecular architecture enables key functions in nature, such as oxygen transport in hemoglobin and light harvesting in chlorophyll, and inspires cutting-edge applications in chemical sensing, catalysis, renewable energy conversion, and optoelectronics. Consequently, significant efforts are dedicated to develop their solution-phase chemistry, particularly by strategically modifying the macrocyclic structure to tailor their properties. Inspired by the field of on-surface covalent synthesis, we introduce a pioneering strategy to tailor porphyrin macrocycles at interfaces, specifically expanding an 18-π porphyrin into a 20-π system. Such transformation is achieved by depositing a porphyrin precursor, equipped with two trifluoromethyl (-CF_3) functional groups in a trans configuration, onto a hot Ag(111) surface. By combining scanning probe microscopy and spectroscopy, complemented with density-functional theory calculations, we confirm the successful formation of the 20-π free-base expanded porphyrin, exhibiting potential high antiaromaticity attributed to the preservation of planar conformation at the interface according to theoretical calculations. The transformation occurs through precursor dehalogenation and subsequent insertion of two carbon atoms into the macrocycle, driving its expansion, and affording a narrow bandgap of ~0.2 eV. Furthermore, we demonstrate its coordinative capabilities toward cobalt, forming a unique two-fold coordination node within the expanded core. Our findings pave the way for engineering expanded porphyrins at interfaces enabling enhanced antiaromaticity and narrow bandgaps, while affording the design of novel coordination motifs, and, simultaneously, demonstrating the capabilities of surface science in exploring such expanded macrocyclic architectures at the atomic scale.

1 | Introduction

Porphyrins are multifunctional macrocyclic compounds, essential to life and technology alike. Their tunable electronic properties make them valuable compounds in materials science, medicine, and renewable energy applications. Furthermore, due to their chemical versatility, photophysics, and ability to coordinate metal ions they have also been used for gas sensing and catalysis [1]. In biological systems, they are integral to heme proteins such as hemoglobin, myoglobin and cytochromes, which are involved in oxygen transport, storage, and electron transfer [2, 3], respectively, while they also form the core of chlorophyll in

Ana Barragán, Elena Pérez-Elvira, Alba García-Frutos, and Diego J. Vicent contributed equally to this work.

photosynthesis [3, 4]. In addition, they are widely used as contrast agents for magnetic resonance imaging in medical applications [5]. In artificial systems, porphyrins are utilized in organic semiconductors, solar cells and light emitting diodes (OLEDs), due to their strong absorption and emission in the visible regime [6, 7]. Additionally, they serve as key building blocks in sensors for detecting gases, volatile compounds, heavy metals and biomolecules, thanks to their sensitivity and specificity [8]. Their catalytic properties also enable them to mimic natural enzymes and facilitate a wide range of chemical reactions [9, 10]. Notably, porphyrins have recently emerged as promising candidates for energy storage, including advanced batteries and fuel cells [11].

Since the suggestion of the porphyrin macrocyclic arrangement more than a century ago [12], the design of porphyrinoids has attracted significant research interest, particularly through solution-phase chemistry [1]. An emerging theme in porphyrinoid chemistry is the deliberate induction and study of antiaromaticity, particularly within expanded macrocycles. By increasing the π-electron count beyond the classic 18-π framework, expanded porphyrins can access 4n π-electron circuits that destabilize the ring's electron delocalization, leading to characteristic paratropic ring currents and unique redox and optical behaviors. Harnessing antiaromaticity in these larger porphyrinoids not only offers a route to tune their frontier orbital energies and reactivity profiles, but also opens new avenues for applications in molecular switches, responsive sensors, and catalysts with unconventional optoelectronic properties [13–16].

In the past two decades, a new discipline of chemistry has emerged, on-surface covalent synthesis, which leverages the chemical reactivity of molecular species on surfaces under ultra-high vacuum (UHV) environment [17–24]. Importantly, such approach allows for the atomic-scale characterization of the reaction products using surface science techniques [25]. Through this methodology, unique molecular products have been synthesized, typically inaccessible in solution chemistry, largely due to concomitant solubility challenges. The list of such products continues to grow exponentially, encompassing nanographenes, one-dimensional molecular wires, nanoribbons, and two-dimensional covalent networks [17–24].

Recognizing the significance of porphyrins, the surface science community, particularly since the advent of scanning probe microscopies, has extensively explored the deposition, adsorption, geometrical conformation, self-assembly, metalation, gas ligation, catalysis and on-surface synthesis of porphyrin derivates [26–28]. However, despite such enormous effort, the synthetic transformations of porphyrin macrocycles at interfaces remains elusive, with reported chemical modifications limited to peripheral transformations or polymerization [29–37]. Indeed, a long-standing goal has been to induce skeletal rearrangement of porphyrinoid precursors at interfaces to promote enhanced antiaromaticity [13, 15, 38].

In this manuscript, we introduce a pioneering on-surface synthesis protocol to transform a prototypical porphyrin macrocycle, expanding it from an aromatic 18-π core (**1**) to an antiaromatic 20-π vinylogous porphyrin (**2**). To this aim, an ABAB-type porphyrin was rationally designed and synthesized, incorporating anthracenyl substituents and trifluoromethyl ($-CF_3$) groups at the *meso* positions in a trans configuration (**1**). Upon deposition on Ag(111) held at 200–300 °C, this precursor undergoes dehalogenation, inserting the remaining carbon atoms from the *gem*-trihalide functional group to form two vinylene bridges within the macrocycle. Concurrently, four oxidative ring closures at the anthracenyl substituents extend the π-conjugation of the lateral moiety, yielding the expanded porphyrin (**2**). Our scanning probe microscopy study, complemented by density functional theory calculations, elucidates the structure and electronic properties of the expanded porphyrin, revealing a remarkably low bandgap of ~0.2 eV. Notably, our theoretical simulations signal the expression of enhanced antiaromaticity reaching a value of 19.0 ppm for NICS(0). The production of **2** coexists with distinct reaction products, including extra hydrogenated (**2′**) or doubly extra hydrogenated 20-π expanded porphyrins (**2″**), as well as π-extended tetrapyrroles with distinct degrees of dehalogenation and hydrogen passivation (**3**, $\mathbf{3_1}$, and $\mathbf{3_2}$), alongside with ethynylene-linked π-extended porphyrin wires (**4**). Notably, such porphyrin expansion is precluded on Au(111), where only individual species and polymers preserving the intact macrocycle are found. Finally, inspired by such unique chemical cavity at interfaces, the capabilities towards metallation of the porphyrinoid were explored, revealing the transformation from the free-base form to Co-metallated species via a distinct two-fold nitrogen-cobalt coordination. Our findings establish a seminal strategy to transform porphyrins at interfaces, demonstrating in particular how to enlarge π-conjugation in large macrocycles and potentially expressing antiaromaticity, while enabling atomistic-scale investigation of their structure and electronic properties.

2 | Results and Discussion

The main idea behind the design of the initial molecular precursor was to endow a porphyrin macrocycle with two *gem*-trifluoride functional groups, each of them at the meso positions and in a trans configuration, as depicted in Scheme 1, pursuing the full dehalogenation and insertion of remaining carbon atoms from the $-CF_3$ groups into the porphyrin macrocycle. Such strategy was fuelled by recent findings on the carbon rearrangement of acenes and sumanenes functionalized with *gem*-dibromide moieties at interfaces [39, 40], as well as on free-base porphyrins in solution [41]. To this end, a CF_3-substituted dipyrromethane was condensed with anthracene-9-carbaldehyde, thereby extending the π-conjugation, under standard conditions for ABAB-porphyrin synthesis (see Figures S1–S4 for synthetic and characterization details of precursor **1**).

Following such strategy, sublimation of a submonolayer coverage of compound **1** on an Ag(111) surface held at 200 °C resulted in the formation of distinct reaction species. The products were elucidated thanks to the combination of scanning tunneling microscopy (STM) and non-contact atomic force microscopy (nc-AFM), complemented by theory [42], as it will be discussed below (cf. Scheme 1, Figures 1a, and S5). All the reaction products have undergone four cyclodehydrogenation reactions of their anthracenyl substituents, being the difference between them the nature of the macrocycle and the two $-CF_3$ moieties upon reaction on the surface. Additionally, a fraction of porphyrin wires was also detected. A completely different scenario emerges upon the deposition of **1** while the Ag(111) substrate is held at room temperature

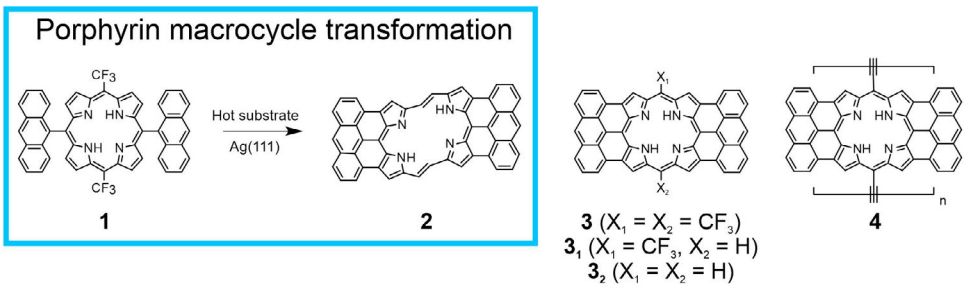

SCHEME 1 | Chemical scheme of the on-surface transformation of precursor **1** into the 20-π expanded porphyrin **2**, and reaction products **3, 3_1, 3_2** and **4**.

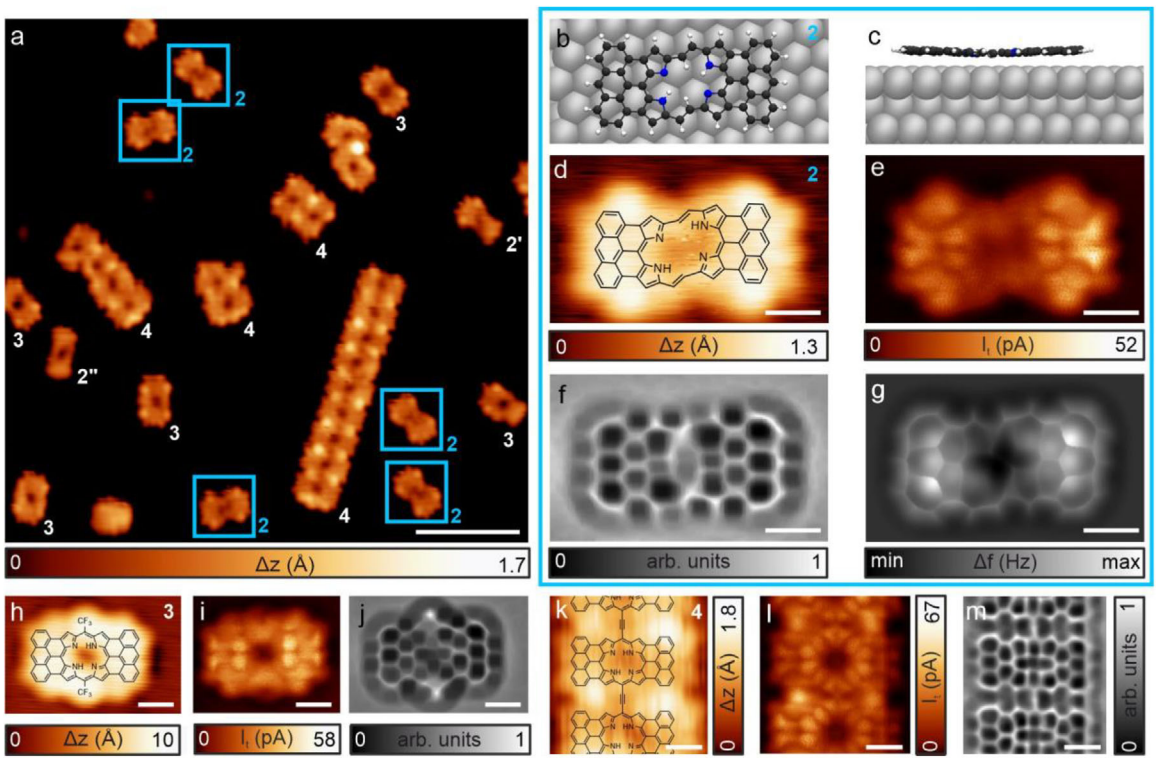

FIGURE 1 | On-surface synthesis of the 20-π expanded porphyrin (**2**), alongside concomitant reaction products by depositing precursor **1** on a Ag(111) substrate held at 200 °C. (a) Overview STM image after deposition of precursor **1** on an Ag(111) substrate held at 200 °C. The different transformed expanded porphyrin species identified are marked by the blue squares. V_b = 50 mV, I_t = 50 pA, scale bar = 4.0 nm. (b, c) Top and side views of the adsorption geometry simulated by DFT of the transformed species **2**, respectively. (d, e) Constant-current (with chemical sketch superimposed. V_b = 500 mV, I_t = 50 pA, scale bar = 5 Å) and constant-height (V_b = 5 mV, scale bar = 5 Å) STM images, respectively, of the transformed 20-π expanded porphyrin **2**. (f, g) Laplace-filtered constant-height frequency-shift nc-AFM image (Z-offset: 150 pm above STM set point: 5 mV, 50 pA. Scale bar = 5 Å), acquired with a CO-functionalized tip, and corresponding calculated frequency-shift image, of species **2**. (h–j) Constant-current STM (V_b = -100 mV, I_t = 50 pA, scale bar = 5 Å), constant-height STM (V_b = 5 mV, scale bar = 5 Å nm), and Laplace-filtered constant-height frequency-shift nc-AFM (Z-offset: 100 pm above STM set point: 5 mV, 50 pA) images of species **3**, respectively. (k-m) Constant-current STM (V_b = 500 mV , I_t = 50 pA, scale bar = 5 Å), constant-height STM (V_b = 5 mV, scale bar = 5 Å), and Laplace-filtered constant-height frequency-shift nc-AFM (Z-offset: 140 pm above STM set point: 5 mV, 50 pA) images of a section of oligomer **4**.

and subsequently annealed to 200 °C, resulting in self-assembled islands and amorphous nanostructures, respectively (cf. Figure S6).

The simulated adsorption geometry of the transformed species **2** is displayed in Figures 1b,c revealing a flat adsorption. Experimental high-resolution STM and nc-AFM images of compound **2** (cf. Figure 1d–f), as well as apparent size comparison of the distinct compounds (cf. Figure S7), reveals the formation of a 20-π vinylogous (2.1.2.1) porphyrin, unprecedented at interfaces. The agreement between experimental (cf. Figure 1f) and simulated nc-AFM images (cf. Figure 1g from the calculated geometry in Figure 1b) is excellent, ratifying a flat adsorption. Here, the vinylene bridge is difficult to be resolved and only comparison

with theoretical simulations allows to discern its presence. Importantly, such simulations highlight the preservation of the pristine pyrrolic rings, i.e., no loss of hydrogen atoms from the macrocycle (cf. Figure 1b) and plausible expression on the surface of the two expected tautomers, which are indistinguishable in this case with our techniques (cf. Figure S8). Alongside these findings, the minor singly and doubly hydrogenation of species **2** at the termini of the extended π-backbone are detected, giving rise to compounds **2′** and **2″** (cf. Figure S5b and S5c).

Concurrently, compound **3** is observed and assigned to the planarization and cyclodehydrogenation on Ag(111) of the initial precursor **1**, which then forms a π-extended porphyrin that has retained its -CF_3 moieties (cf. Figures 1h–j). Regarding the macrocycle, high resolution nc-AFM imaging at distinct heights reveals its preservation, without coordination with surface adatoms (cf. Figure S9). Illustrating the reaction evolution of such species, compounds $\mathbf{3_1}$ and $\mathbf{3_2}$ result from the subsequent loss of one or two -CF_3 moieties, respectively (cf. Figure S5e and S5f), followed by hydrogen passivation.

Additionally, we detect the formation of one-dimensional wires (**4**), whose monomers are simply the above-mentioned π-extended porphyrins, which upon dehalogenation, they have engaged in homocoupling, being bridged through ethynylene bonds (cf. Figures 1k–m and S5g), thus reproducing the on-surface reactivity of *gem*-polyhalide functional groups previously reported for acene, periacene, and porphyrin derivates [22, 43–50].

In order to investigate the role of the substrate in the chemical reactivity of compound **1**, we examined two key factors: the substrate temperature upon species arrival and the nature of the substrate itself. By controlling the substrate temperature, we were able to tune the formation of distinct species (cf. Figure S10), achieving a maximum yield of (16,0 $\pm$ 1.2) for compounds **2**, **2′** and **2″** after deposition with the Ag(111) surface held at 300 °C, coexisting with **3**, $\mathbf{3_1}$ and $\mathbf{3_2}$ (27.1 $\pm$ 1.5) and **4** (29.2 $\pm$ 1.5) %. Additionally, conducting experiments on Au(111) we prevented the expansion of porphyrins, i.e. we precluded the formation of compound **2**, highlighting the crucial role of Ag(111) in enabling this unique interfacial reactivity of porphyrins (Figure S11).

In the search for a deeper understanding of the reaction mechanisms for the transformation of the 18-π core porphyrin (**1**) into the 20-π porphyrin (**2**), we performed a series of Quantum Mechanics/Molecular Mechanics (QM/MM)-based Molecular dynamics (MD) simulations [51]. Experimentally, we detected the survival of -CF_3 in fully planarized species (**3** and $\mathbf{3_1}$, cf. Figure S7), indicating that cyclodehydrogenation precedes dehalogenation. Computationally, we found that the most likely scenario after the dehalogenation of the -CF_3 is the incorporation of the remaining carbons into the macrocycle. We propose a six-step reaction mechanism, for the two carbon insertions into the macrocycle, where the first three steps (shown in Figure 2) are analogous to the last three (displayed in Figure S12).

First, the carbon from the -CF_3 moiety after the dehalogenation, likely assisted by an Ag adatom that passivates it [39, 40] is inserted in the macrocycle, overcoming an energy barrier of 1.44 eV. Subsequently, molecular hydrogen would reduce the alkynyl bridge into alkenyl [41]. This two-step process will implicate two free energy barriers of 1.35 eV and 0.62 eV, taking the system to a state 1.75 eV more favorable than the initial configuration. Once the Ag adatom that participated in the process is no longer chemically bonded to the molecule, we assumed it can easily diffuse away from the molecule. To complete the 18-π into 20-π porphyrin transformation, a similar process would occur in the opposite side of the molecule. The second part of the process, shown in the Figure S12, would implicate a similar mechanism and three energy barriers of 0.93 , 1.64 , and 0.83 eV. After the two described reaction pathways, the exothermic transformation of the 18-π core (**1**) porphyrin into the 20-π porphyrin (**2**) would be completed, having liberated 3.75 eV of free energy in the process. A chemical sketch of the complete process is shown in Figure S13.

Next, given its novelty and significance at interfaces, we focus on the electronic structure of the 20-π expanded porphyrin (**2**). First of all, we paid attention to the potential antiaromatic character of the species. To this aim, NICS(0) calculations [52] reveal an enhanced value of 19.0 ppm highlighting a potential antiaromatic ring within 20-π core (cf. Figure 3a). In addition, the values for the π-extended planarized termini signal aromatic currents. Further evidence for antiaromaticity is provided by the experimental bond-length pattern along the periphery of the porphyrinoid 20-π pathway, which agrees well with theoretical simulations (cf. Figure S14). It is important to note that ideal antiaromaticity is never observed experimentally, as such systems tend to alleviate electronic destabilization typically through bond length alternation, as found here in some sections of the path, while still preserving a paratropic current [53–55]. Future experiments enabling direct ring-current measurements would be valuable to corroborate the antiaromatic character of species **2**.

While numerous expanded porphyrins have been synthesized [13, 15, 26, 38], only a subset have been characterized as antiaromatic species [38, 41]. This is because antiaromatic 4n π-electron counts are generally avoided through conformational distortions (e.g., Möbius aromaticity) or redox/topological modifications [38]. A seminal example of genuine antiaromaticity is *trans*-[20]porphyrin(2.1.2.1) [41, 56], a macrocycle structurally related [38, 41, 56–59] to compound **2**, which exhibits a solution-phase NICS(0) value of 16.63 ppm. To evaluate planarity, we compared the mean deviation from the molecular plane in both compounds. [20] porphyrin(2.1.2.1) shows a deviation of 0.052 Å, while our compound **2**, adsorbed on Ag(111), exhibits a deviation of 0.09 Å, both indicating highly planar structures. Thus, our findings underscore the potential of on-surface synthesis to yield and stabilize planarized expanded antiaromatic porphyrins on surfaces.

Intrigued by the expected low bandgap of such antiaromatic species **2**, we performed scanning tunneling spectroscopy (STS) at selected positions of the species, which reveals a pronounce resonance starting close to Fermi in the positive bias regime (unoccupied states), without any other relevant fingerprint (cf. Figure 3b). To circumvent such limitation, we carried out dI/dV mapping at selected voltage biases from -0.65 V to 0.65 V (cf. Figure S15), identifying the frontier orbitals at −0.15 V and 0.05 V, resulting in a bandgap of ∼0.2 eV. The nice agreement between

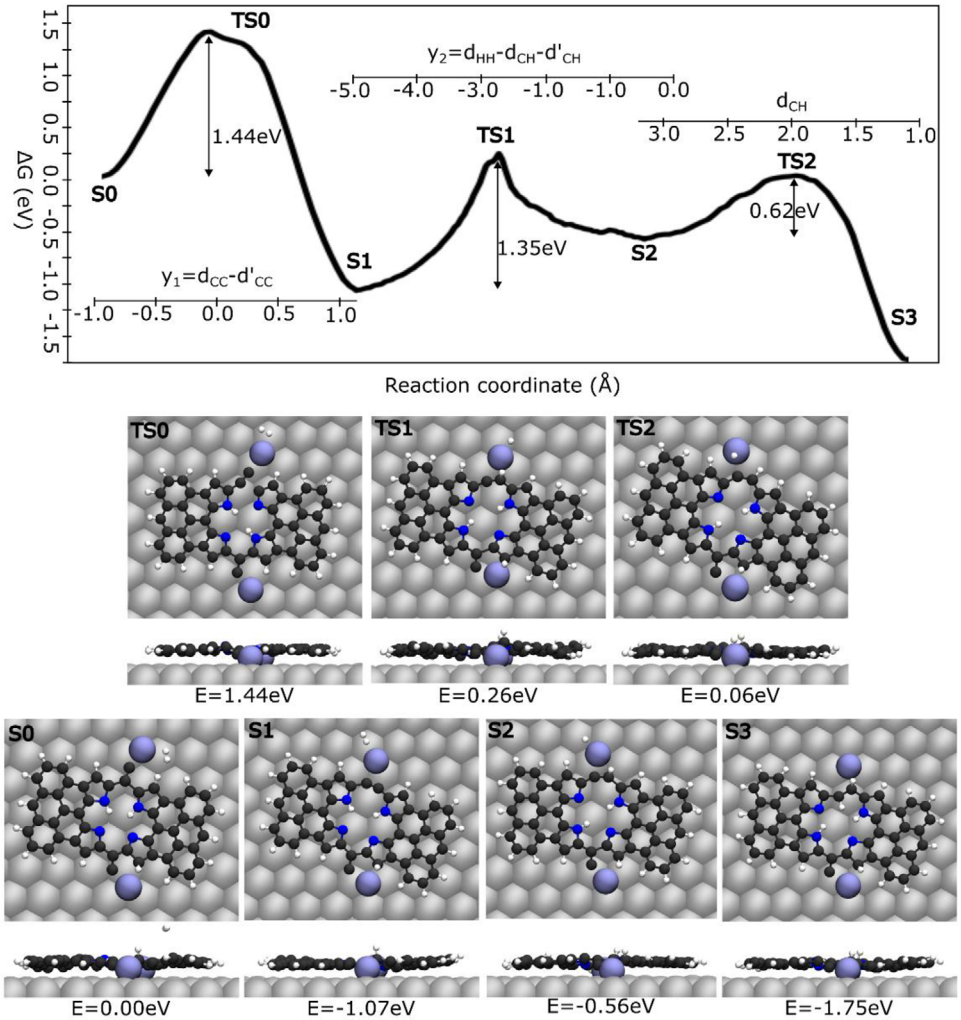

FIGURE 2 | First three steps of the reaction mechanism for the incorporation of a carbon atom into the porphyrin backbone upon deposition of **1** on a Ag(111) substrate held at 200 °C and subsequent dehalogenation of -CF_3 moieties. Free energy profile of the first three steps of the reaction mechanism proposed for the transformation of **1** into **2**, calculated within the QM/MM formalism. The analogous three-step process that completes the transformation of **1** into **2** can be found in the Figure S12. The reaction coordinates specified for the three steps are: (1) $y_1 = d_{CC} - d'_{CC}$, where d_{CC} is the distance between the two C atoms which are forming the bond we break and d'_{CC} the distance between the two carbons that create the new bond. (2) $y_2 = d_{HH} - d_{CH} - d'_{CH}$, where d_{HH} is the distance between the H atoms in the H_2 used for reducing the alkynyl bridge into alkenyl, and d_{CH}, d'_{CH} are the distances between the H atoms and the C atoms to be reduced. (3) d_{CH}, which is the distance between the H and C atoms that remain to create the bond.

experimental and theoretical dI/dV maps corroborated our rationalization of the electronic structure (cf. Figures 3c–f). Based on these findings and the absence of a Kondo resonance near the Fermi level (cf. Figure S15), typically associated with an unpaired electron delocalized over the π-system, we rule out any significant molecule–substrate charge transfer. Importantly, such narrow value for the bandgap could be related to the pronounced antiaromaticity calculated in species **2**, since antiaromatic compounds inherently exhibit small bandgaps, underscoring the potential use of the reported species in optoelectronic applications where efficient low-energy transitions are critical.

Finally, we inspected the coordination capabilities [27, 28, 60, 61] of the 20-π expanded porphyrin (**2**) at the atomic scale, selecting cobalt due to its strong propensity to metallate porphyrinoids. To this aim, we first deposited precursor **1** on Ag(111) held at 300°C and, subsequently, expose it to a flux of cobalt atoms (see overview in Figure S16). Our inspection allows, in such a way, not only to assess the potential metallation of the expanded porphyrins, but also to provide an atomistic insight on the propensity of distinct porphyrinoids for coordinating with 3d metals.

As illustrated by STM and nc-AFM imaging (cf. Figures 4a–c), the metallation of **2** was successful, which is evidenced by the presence of a protrusion in the cavity by STM and a cross-like feature by nc-AFM, thus affording a two-fold coordinated species **2-Co** with a yield of metallation of 21 ± 5% (cf. Figures S16 and S17). The calculated optimized geometry of **2-Co** (cf. Figure 4d) highlights that the cobalt node is coordinated through two iminic nitrogen atoms, while still two pyrrolic rings are present (see Figure S18 for discarded dehydrogenation and metallation of compound **2** tautomer). Metallation of residual **2′** and **2″** species, giving rise to **2′-Co** and **2′-Co** was also successful as illustrated in Figure S17.

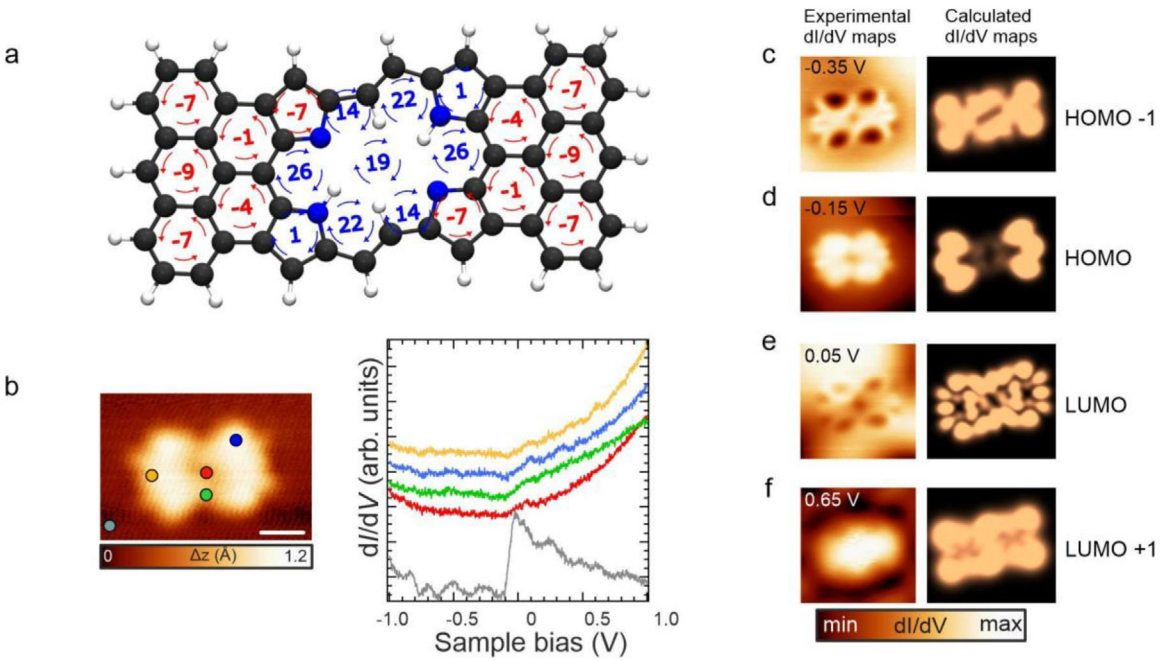

FIGURE 3 | Antiaromaticity calculations and electronic characterization of **2** on Ag(111). (a) NICS(0) calculation of **2**. NICS(0) positive (negative) values indicate antiaromatic (aromatic) character. To facilitate the interpretation of the NICS(0) values we plotted the positive (negative) in blue (red) and added clock-(counter clock-)wise arrows, based on their relation to the induced magnetic current density. (b) Long-range dI/dV spectra (right panel) acquired on the positions indicated by colours in the topographic STM image (left panel). Reference spectrum (gray) was taken on the Ag(111) surface. V_b = -0.35 V, I_t = 250 pA. Open feedback parameters for dI/dV spectra: V_b = -1.0 V, I_t = 400 pA, V_{rms} = 30 mV. (c–f) Experimental constant-current differential conductance maps (left panels, I_t = 50 pA), taken at the energies indicated within each map (−0.35 V, −0.15 V, 0.05 V, 0.65 V), and simulated dI/dV maps (right panels) of **2**.

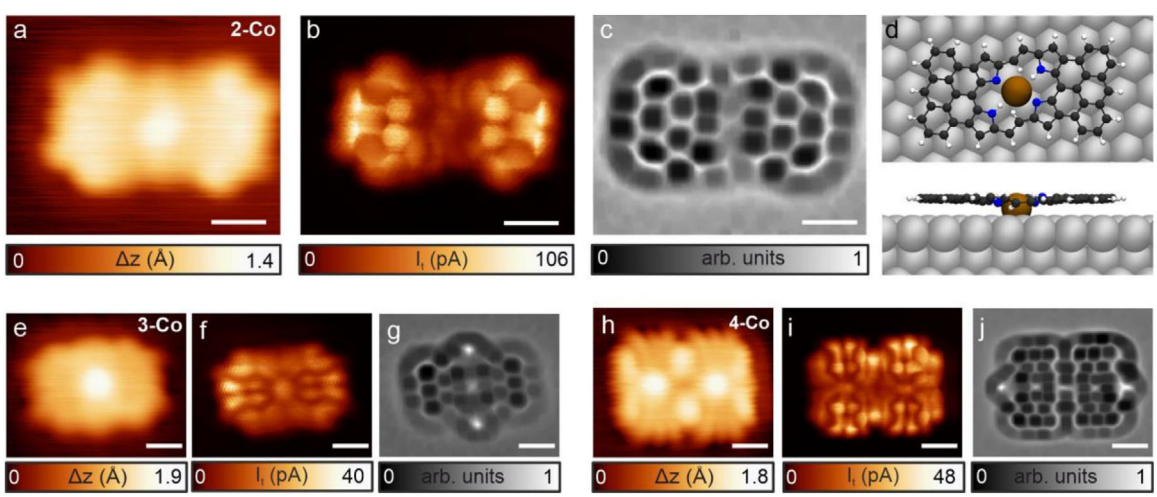

FIGURE 4 | Metallation of 20-π (2.1.2.1) porphyrin on Ag(111) by cobalt. Scanning probe microscopy of distinct products obtained after deposition of precursor **1** on Ag(111) substrate held at 300°C and dosing of Co atoms for 4 min. (a, b) Constant-current (V_b = 0.5 V, I_t = 30 pA, scale bar = 5 Å) and constant-height (V_b = 5 mV, scale bar = 5 Å) STM images of the Co-metallated transformed 20-π expanded porphyrin, **2-Co**. (c) Corresponding experimental Laplace-filtered constant-height frequency-shift nc-AFM image, acquired with a CO functionalized tip (Z-offset: 145 pm above STM set point: 5 mV, 50 pA. Scale bar = 5 Å). d) Top and side view of the DFT simulation of the relaxed geometry of **2-Co** on Ag(111). (e–g) Constant-current STM (V_b = 0.5 V, I_t = 50 pA, scale bar = 5 Å), constant-height STM (V_b = 5 mV, scale bar = 5 Å), and Laplace-filtered constant-height frequency-shift nc-AFM (Z-offset: 160 pm above STM set point: 5 mV, 50 pA) images of the species **3** metallated with Co, **3-Co**, respectively. (h–j) Constant-current STM (V_b = 0.5 V, I_t = 50 pA, scale bar = 6 Å), constant-height STM (V_b = 5 mV, scale bar = 6 Å), and Laplace-filtered constant-height frequency-shift nc-AFM (Z-offset: 200 pm above STM set point: 5 mV, 50 pA) images of a metallated oligomer **4-Co**.

Concomitantly, we observed the metallation of different products formerly coexisting with compound **2**, leading to the formation of **3-Co, 3_1-Co** and **3_2-Co** (cf. Figures 4e–g and S17), as well as **4-Co** oligomers (cf. Figures 4h–j and S17). These species are readily identified by the appearance of a protrusion within the cavities, analogous to that observed in the previously characterized **2-Co**. A statistical analysis of 253 species enabled us to evaluate the metallation propensity (Figure S16), revealing average yields of $(70 \pm 5)\%$ for **3-Co, 3_1-Co** and **3_2-Co**, and $(93 \pm 5)\%$ for **4-Co**, both higher than for **2-Co**. The enhanced tendency for metallation in the archetype tetrapyrrole-based species, compared to the π-expanded transformed compound **2,** likely stems from the increased cavity size in **2**. In such expanded macrocyclic, the two pyrrolic nitrogen atoms lie 2.1 Å from the cobalt centre, whereas the two iminic nitrogen atoms are 3.1 Å away (cf. Figure S18), significantly further than in a typical porphyrin, thus reducing the overall metallation rate.

3 | Conclusions

In this work, we present a pioneering on-surface synthesis strategy to expand a prototypical porphyrin macrocycle from an 18-π aromatic system to a 20-π antiaromatic vinylogous porphyrin, enlarging the π-conjugation pathway. This transformation, achieved through dehalogenation and subsequent carbon insertion from trifluoromethyl functional groups at the meso positions in a trans configuration, successfully extends the π-conjugation of the macrocyclic core. By employing scanning probe microscopy and spectroscopy, complemented with density functional theory calculations, we unambiguously identified the structure and electronic properties of the expanded porphyrin, revealing a narrow bandgap of ~0.2 eV and a pronounced antiaromatic character according to NICS calculations. Our findings underscore the critical role of the Ag(111) surface in directing this transformation, contrasted by the absence of product formation on Au(111), as well as the importance of elevated substrate temperatures during precursor sublimation to enhance the yield of the desired product. Notably, the surface not only stabilizes the expanded species, but also preserves a planarized geometry, which is essential for sustaining the enhanced antiaromaticity observed. We further demonstrate the successful metallation of the 20-π system with cobalt, yielding a unique metallated complex featuring two-fold nitrogen-cobalt coordination, and importantly steering new paths for exploring coordination environments with submolecular resolution.

These findings open new avenues for the controlled synthesis of expanded porphyrins on surfaces, providing a versatile approach for tailoring their electronic, antiaromatic and coordination characteristics. The implications of our work extend beyond fundamental surface chemistry, offering potential applications in organic electronics, energy conversion, and catalysis. Furthermore, the observed substrate-dependent reactivity underscores the importance of interfacial interactions in on-surface synthesis, paving the way for the rational design of surface-mediated molecular transformations. We envision future studies will leverage this strategy to explore expanded macrocyclic systems, thus enriching the field of functional organic materials, particularly those ones displaying unique features such as antiaromaticity.

Author Contributions

The manuscript was written through contributions of all authors. All authors have given approval to the final version of the manuscript.

Acknowledgments

The authors acknowledge to several funding organizations for their financial support. We thank funding from the Agencia Estatal de Investigacion (AEI) PID2019-108532GB-I00, PID2023-146373OB-I00, and PID2022-136961NB-I00. We acknowledge support from QUIMTRONIC-CM Y2018/NMT-4783, the '(MAD2D-CM)-IMDEA-Nanociencia' and '(MAD2D-CM)-UCM' projects funded by Comunidad de Madrid, by the Recovery, Transformation and Resilience Plan, and by NextGenerationEU from the European Union. The authors thank Comunidad de Madrid through Programa de Actividades de I+D (TEC-2024/TEC-459, SYNMOLMAT-CM; and MOLQUANTUM-CM SYG-2024/TEC-707). IMDEA Nanociencia is appreciative of support from the "Severo Ochoa" Programme for Centers of Excellence in R&D (CEX2020-001039-S). N.M. and D.J.-V. acknowledge the financial support by the ERC (SyG TOMATTO ERC-2020 951224), and D.E. and A.B. by the ERC (SyG MAGNESIS ERC-2024 101224406). A.B. and A.G. thank financial support from Juan de la Cierva program. A.G. acknowledges the financial support from the IDEAL postdoctoral MSCA-cofund. The authors acknowledge Dr. Jorge Labella for fruitful discussions.

Conflicts of Interest

The authors declare no conflicts of interest.

Data Availability Statement

The Data That Support the Findings of this Study Are Available from the Corresponding Author Upon Reasonable Request

References

1. M. O. Senge, N. N. Sergeeva, and K. J. Hale, "Classic Highlights in Porphyrin and Porphyrinoid Total Synthesis and Biosynthesis," *Chemical Sociecty Revise* 50 (2021): 4730–4789.

2. H. L. Bonkovsky, J. Guo, W. Hou, T. Li, T. Narang, and M. Thapar, "Porphyrin and Heme Metabolism and the Porphyrias. Comprehensive Physiology," *Comprehensive Physiology* 3 (2013): 365–401.

3. A. R. Battersby, "Tetrapyrroles: The Pigments of Life," *Natural Product Reports* 17 (2000): 507–526.

4. D. Mauzerall, In *Photosynthesis I: Photosynthetic Electron Transport and Photophosphorylation*, ed. A. Trebst, and M. Avron, (Springer, 1977): 117–124.

5. V. Nikolaou, E. Nikoloudakis, K. Ladomenou, G. Charalambidis, and A. G. Coutsolelos, *Front Chem Biol* 2 (2024): 1346465.

6. A. Mahmood, J. Hu, B. Xiao, A. Tang, X. Wang, and E. Zhou, "Recent Progress in Porphyrin-based Materials for Organic Solar Cells," *Journal of Materials Chemistry A* 6 (2018): 16769–16797.

7. M. Urbani, G. de la Torre, M. K. Nazeeruddin, and T. Torres, "Phthalocyanines and Porphyrinoid Analogues as Hole- and Electron-transporting Materials for Perovskite Solar Cells," *Chemical Society Review* 48 (2019): 2738–2766.

8. R. Paolesse, S. Nardis, D. Monti, M. Stefanelli, and C. Di Natale, "Porphyrinoids for Chemical Sensor Applications," *Chemical Review* 117 (2017): 2517–2583.

9. B. Meunier, "Metalloporphyrins as Versatile Catalysts for Oxidation Reactions and Oxidative DNA Cleavage," *Chemical Review* 92 (1992): 1411–1456.

10. S. Gu, A. N. Marianov, T. Lu, and J. Zhong, "A Review of the Development of Porphyrin-based Catalysts for Electrochemical CO2 Reduction," *Chemical Engineering Journal* 470 (2023): 144249.

11. M. Xie, J. Liu, L. Dai, H. Peng, and Y. Xie, "Advances and prospects of porphyrin derivatives in the energy field," *RSC Advances* 13 (2023): 24699–24730.

12. W. Küster, "Beiträge zur Kenntnis des Bilirubins und Hämins," *Biological Chemistry* 82 (1912): 463–483.

13. J. L. Sessler and D. Seidel, "Synthetic Expanded Porphyrin Chemistry," *Angewandte Chemie International Edition* 42 (2003): 5134–5175.

14. T. Sarma and P. K. Panda, "Annulated Isomeric, Expanded, and Contracted Porphyrins," *Chemical Review* 117 (2017): 2785–2838.

15. S. Saito and A. Osuka, "Expanded Porphyrins: Intriguing Structures, Electronic Properties, and Reactivities," *Angewandte Chemie International Edition* 50 (2011): 4342–4373.

16. T. Tanaka and A. Osuka, "Chemistry of Meso -Aryl-Substituted Expanded Porphyrins: Aromaticity and Molecular Twist," *Chemical Review* 117 (2017): 2584–2640.

17. Q. Shen, H. Gao, and H. Fuchs, "Frontiers of on-surface Synthesis: From Principles to Applications," *Nano Today* 13 (2017): 77–96.

18. S. Clair and D. G. de Oteyza, "Controlling a Chemical Coupling Reaction on a Surface: Tools and Strategies for on-Surface Synthesis," *Chemical Review* 119 (2019): 4717–4776.

19. T. Wang and J. Zhu, "Confined on-surface Organic Synthesis: Strategies and Mechanisms," *Surface Science Reports* 74 (2019): 97–140.

20. Q. Sun, R. Zhang, J. Qiu, R. Liu, and W. Xu, "On-Surface Synthesis of Carbon Nanostructures," *Advanced Materials* 30 (2018): 1705630.

21. L. Talirz, P. Ruffieux, and R. Fasel, "On-Surface Synthesis of Atomically Precise Graphene Nanoribbons," *Advanced Materials* 28 (2016): 6222–6231.

22. J. I. Urgel, A. Sánchez-Grande, D. J. Vicent, P. Jelínek, N. Martín, and D. Écija, "On-Surface Covalent Synthesis of Carbon Nanomaterials by Harnessing Carbon Gem- Polyhalides," *Advanced Materials* 36 (2024): 2402467.

23. B. Yang, B. Dong, and L. Chi, "On-Surface Intramolecular Reactions," *ACS Nano* 14 (2020): 6376–6382.

24. W. Zeng and J. Wu, "Open-Shell Graphene Fragments," *Chemistry (Weinheim An Der Bergstrasse, Germany)* 7 (2021): 358–386.

25. N. Pavliček and L. Gross, "Generation, manipulation and characterization of molecules by atomic force microscopy," *Natural Revision Chemistry* 1 (2017): 0005.

26. W. Auwärter, D. Écija, F. Klappenberger, and J. V. Barth, "Porphyrins at Interfaces," *Nature Chemistry* 7 (2015): 105–120.

27. J. M. Gottfried, "Surface Chemistry of Porphyrins and Phthalocyanines," *Surface Science Reports* 70 (2015): 259–379.

28. K. Diller, A. C. Papageorgiou, F. Klappenberger, F. Allegretti, J. V. Barth, and W. Auwärter, "In Vacuo Interfacial Tetrapyrrole Metallation," *Chemical Society Revision* 45 (2016): 1629–1656.

29. G. Di Santo, S. Blankenburg, C. Castellarin-Cudia, et al., "Supramolecular Engineering Through Temperature-Induced Chemical Modification of 2 H -Tetraphenylporphyrin on Ag(111): Flat Phenyl Conformation and Possible Dehydrogenation Reactions," *Chemical European Journal* 17 (2011): 14354–14359.

30. A. C. Papageorgiou, S. Fischer, S. C. Oh, et al., "Self-Terminating Protocol for an Interfacial Complexation Reaction in Vacuo by Metal–Organic Chemical Vapor Deposition," *ACS Nano* 7 (2013): 4520–4526.

31. A. Wiengarten, K. Seufert, W. Auwärter, et al., "Surface-assisted Dehydrogenative Homocoupling of Porphine Molecules," *Journal of the American Chemical Society* 136 (2014): 9346–9354.

32. A. Wiengarten, J. A. Lloyd, K. Seufert, et al., "Surface-Assisted Cyclodehydrogenation; Break the Symmetry, Enhance the Selectivity," *Chemical European Journal* 21 (2015): 12285–12290.

33. Q. Sun, L. M. Mateo, R. Robles, et al., "Inducing Open-Shell Character in Porphyrins Through Surface-Assisted Phenalenyl π-Extension," *Journal of the American Chemical Society* 142 (2020): 18109–18117.

34. Q. Sun, L. M. Mateo, R. Robles, et al., "Bottom-Up Fabrication and Atomic-Scale Characterization of Triply Linked, Laterally π-Extended Porphyrin Nanotapes**," *Angewandte Chemie International Edition* 60 (2021): 16208–16214.

35. M. Tenorio, M. Lozano, L. Cerna, et al., "Coordinative Self-assembly of -Electron Magnetic Porphyrins," *Angewandte Chemie International Edition* 64 (2025): e202420572.

36. Y. Gu, F. Xiang, Y. Liang, et al., "peri-Fused Porphyrin Edges," *Angewandte Chemie International Edition* 64 (2025): e202417129.

37. E. C. Rascon, A. Riss, A. Matěj, et al., "On-Surface Synthesis of Square-Type Porphyrin Tetramers With Central Antiaromatic Cyclooctatetraene Moiety," *Journal of the American Chemical Society* 145 (2023): 967–977.

38. J. L. Sessler, Z. Gross, and H. Furuta, "Introduction: Expanded, Contracted, and Isomeric Porphyrins," *Chemical Revision* 117 (2017): 2201–2202.

39. E. Pérez-Elvira, A. Barragán, Q. Chen, et al., "Generating Antiaromaticity in Polycyclic Conjugated Hydrocarbons by Thermally Selective Skeletal Rearrangements at Interfaces," *Natural Synthesis* 2 (2023): 1159–1170.

40. E. Pérez-Elvira, A. Barragán, A. Gallardo, et al., "Coronene-Based 2D Networks by On-Surface Skeletal Rearrangement of Sumanene Precursor," *Angewandte Chemie International Edition* 64 (2025): e202414583.

41. M. Umetani, T. Tanaka, T. Kim, D. Kim, and A. Osuka, "Double Ring Expansion From an Aromatic [18]Porphyrin(1.1.1.1) to an Antiaromatic [20]Porphyrin(2.1.2.1)," *Angewandte Chemie International Edition* 55 (2016): 8095–8099.

42. N. Oinonen, A. V. Yakutovich, A. Gallardo, M. Ondráček, P. Hapala, and O. Krejčí, "Advancing Scanning Probe Microscopy Simulations: A Decade of Development in Probe-particle Models," *Computer Physics Communications* 305 (2024): 109341.

43. S. Kawai, A. Ishikawa, S. Ishida, et al., "On-Surface Synthesis of Porphyrin-Complex Multi-Block Co-Oligomers by Defluorinative Coupling," *Angewandte Chemie International Edition* 61 (2022): e202114697.

44. A. Sánchez-Grande, B. de la Torre, J. Santos, et al., "On-Surface Synthesis of Ethynylene-Bridged Anthracene Polymers," *Angewandte Chemie International Edition* 58 (2019): 6559–6563.

45. A. Sánchez-Grande, J. I. Urgel, I. García-Benito, et al., "Surface-Assisted Synthesis of N - Containing π -Conjugated Polymers," *Advancement of Science* 9 (2022): 2200407.

46. A. Sánchez-Grande, J. I. Urgel, A. Cahlík, et al., "Diradical Organic One-Dimensional Polymers Synthesized on a Metallic Surface," *Angewandte Chemie International Edition* 59 (2020): 17594–17599.

47. B. de la Torre, A. Matěj, A. Sánchez-Grande, et al., "Tailoring π-conjugation and Vibrational Modes to Steer on-surface Synthesis of Pentalene-bridged Ladder Polymers," *Nature Communications* 11 (2020): 4567.

48. B. Cirera, A. Sánchez-Grande, B. de la Torre, et al., "Tailoring Topological Order and π-conjugation to Engineer Quasi-metallic Polymers," *Nature Nanotechnology* 15 (2020): 437–443.

49. E. Pérez-Elvira, F. Wu, J. H. Hwang, et al., "On-Surface Synthesis of a Naphtho-fused [14]Cyclacene," *Angewandte Chemie International Edition* 64 (2025): e202506803.

50. Z. Wang, B. Qie, W. Tang, et al., "Pseudo–Jahn–Teller Distortion in a One-Dimensional π-Conjugated Polymer," *Journal of the American Chemical Society* 148 (2026): 7723–7730.

51. J. I. Mendieta-Moreno, R. C. Walker, J. P. Lewis, P. Gómez-Puertas, J. Mendieta, and J. Ortega, "fireball / Amber: An Efficient Local-Orbital DFT QM/MM Method for Biomolecular Systems," *Journal of Chemical Theory and Computation* 10 (2014): 2185–2193.

52. Z. Chen, C. S. Wannere, C. Corminboeuf, and R. Puchta, "Schleyer Pv. Nucleus-independent chemical shifts (NICS) as an aromaticity criterion," *Chemical Review* 105 (2005): 3842–3888.

53. C. Hong, J. Baltazar, and J. D. Tovar, *European Journal of Organic Chemistry* 2022 (2022): e202101343.

54. R. Lavendomme and M. Yamashina, "Antiaromaticity in Molecular Assemblies and Materials," *Chemical Science* 15 (2024): 18677–18697.

55. M. Baranac-Stojanović, "Aromaticity and Antiaromaticity: How to Define Them," *Chemistry (Weinheim An Der Bergstrasse, Germany)* 7 (2025): 127.

56. D. Kuzuhara and H. Yamada, "Porphyrinoids With Vinylene Bridges," *Synlett* 32 (2020): 1072–1084.

57. D. Kuzuhara, W. Furukawa, A. Kitashiro, N. Aratani, and H. Yamada, "Synthesis and Metalation of Doubly o -Phenylene-Bridged Cyclic Bis(dipyrrin)s With Highly Bent Skeleton of Dibenzoporphyrin(2.1.2.1)," *Chemical European Journal* 22 (2016): 10671–10678.

58. D. Kuzuhara, W. Furukawa, N. Aratani, and H. Yamada, "Cyclic Butadiyne-linked Porphyrin(2.1.2.1) Oligomers," *Journal Porphyr Phthaloc* 24 (2019): 489–497.

59. S. Xue, D. Kuzuhara, N. Aratani, and H. Yamada, *Organic Letters* 21 (2019): 2069.

60. B. Cirera, O. Trukhina, J. Björk, et al., "Long-Range Orientational Self-Assembly, Spatially Controlled Deprotonation, and Off-Centered Metalation of an Expanded Porphyrin," *Journal of the American Chemical Society* 139 (2017): 14129–14136.

61. A. Barragán, M. Urbani, A. Gallardo, et al., "On-Surface Synthesis of Covalently-Linked Carbaporphyrinoid-Based Low-Dimensional Polymers," *Small* 21 (2025): 2408085.

Supporting Information

Additional supporting information can be found online in the Supporting Information section.

Supporting File 1: The following files are available free of charge.

Experimental details for the synthesis. Experimental methods.

Computational details. Supplementary figures.